

Density functional theory calculations of generalized stacking fault energy surfaces for eight face-centered cubic transition metals

Cite as: J. Appl. Phys. **126**, 105112 (2019); <https://doi.org/10.1063/1.5115282>

Submitted: 17 June 2019 . Accepted: 24 August 2019 . Published Online: 12 September 2019

Yanqing Su , Shuzhi Xu , and Irene J. Beyerlein

COLLECTIONS

 This paper was selected as Featured



[View Online](#)



[Export Citation](#)



[CrossMark](#)



Instruments for Advanced Science

Contact Hiden Analytical for further details:
W www.HidenAnalytical.com
E info@hiden.co.uk

CLICK TO VIEW our product catalogue



Gas Analysis

- dynamic measurement of reaction gas streams
- catalysis and thermal analysis
- molecular beam studies
- dissolved species probes
- fermentation, environmental and ecological studies



Surface Science

- UHV TPD
- SIMS
- end point detection in ion beam etch
- elemental imaging - surface mapping



Plasma Diagnostics

- plasma source characterization
- etch and deposition process reaction kinetic studies
- analysis of neutral and radical species



Vacuum Analysis

- partial pressure measurement and control of process gases
- reactive sputter process control
- vacuum diagnostics
- vacuum coating process monitoring

Density functional theory calculations of generalized stacking fault energy surfaces for eight face-centered cubic transition metals

Cite as: J. Appl. Phys. 126, 105112 (2019); doi: 10.1063/1.5115282

Submitted: 17 June 2019 · Accepted: 24 August 2019 ·

Published Online: 12 September 2019



View Online



Export Citation



CrossMark

Yanqing Su,^{1,a)}  Shuzhi Xu,²  and Irene J. Beyerlein³

AFFILIATIONS

¹ Department of Mechanical Engineering, University of California, Santa Barbara, Santa Barbara, California 93106-5070, USA

² California NanoSystems Institute, University of California, Santa Barbara, Santa Barbara, California 93106-6105, USA

³ Department of Mechanical Engineering and Materials Department, University of California, Santa Barbara, Santa Barbara, California 93106, USA

^{a)}Author to whom correspondence should be addressed: yanqingsu@ucsb.edu

ABSTRACT

In this work, we use density functional theory to calculate the entire generalized stacking fault energy (GSFE) surface for eight transition metals with a face-centered cubic structure: Ag, Au, Cu, Ir, Ni, Pd, Pt, and Rh. Analysis of the $\langle 112 \rangle$ GSFE curves finds that the displacements corresponding to the unstable stacking fault energy are larger than the ideal value for all eight metals except Ag and Cu. Over the entire surface, Pt is found to not possess well-defined local maxima or minima, suggesting spreading in favor of dissociation of the dislocation core, unlike the other seven metals. Our calculations also reveal that at a large $\langle 112 \rangle$ displacement, where atoms on two $\{111\}$ adjacent planes are aligned, an anomalous local minimum occurs for Ir and Rh. The oddity is explained by relatively large, localized atomic displacements that take place in the two metals to accommodate the alignment that do not occur in the other six metals. In addition to the fully calculated surfaces, we characterize a continuous 11-term Fourier-series function, which provides a particularly excellent representation of the GSFE surfaces for Ag, Au, Cu, Ni, and Pd.

Published under license by AIP Publishing. <https://doi.org/10.1063/1.5115282>

I. INTRODUCTION

Many industrially relevant metals have a face-centered cubic (FCC) crystal structure.^{1,2} The plastic response of FCC metals is governed by the motion of dislocations and deformation twins on specific crystallographic planes.^{3,4} A well-recognized characteristic of dislocations in FCC systems is that their atomic cores can be extended in their glide planes, spanning from a fraction to several tens of nanometers in width, depending on the metal.⁵ In this core region, the dislocation generates a heterogeneous distribution of atomic displacements across the glide plane. The extent of the dislocation core, whether wide or narrow, is fundamental to understanding its mobility and the type of dislocation processes (i.e., cross slip or climb) and plastic deformation mechanisms (wavy slip, deformation twinning) that can be expected to prevail in a given FCC metal.^{6,7} Many studies have been devoted to estimating or characterizing the size of the dislocation core in FCC systems.

Most models or experimental studies interpret the dislocation core as an energetically stable structure.⁸ The total Burgers vector of the dislocation prefers to dissociate into two Shockley partial dislocations with smaller length Burgers vectors,^{9,10} thereby lowering the total strain energy, but at the expense of creating a faulted region, named the intrinsic stacking fault (ISF), in between the partials, which increases the core energy. The excess energy corresponding to the fault is the intrinsic stacking fault energy (ISFE), γ_{isf} . The size of the individual Shockley partial dislocations and the ISF width separating them are considered the two primary structural length scales constituting the dislocation core.¹¹

Due to the fine characteristic length scales of dislocation cores, calculations for core structures usually involve atomic-level simulations. In this class of modeling, *ab initio* techniques can best account for the nonlinear, anisotropic interactions between the core

atoms. However, since the cores of most FCC metals generally span a few nanometers, application of density functional theory (DFT) would be too computationally intensive. One exception is Al, which has a narrow core and for which a number of studies have used full DFT calculations,^{12,13} reporting ISF widths in the range of 0.66–1.28 nm. For other pure FCC metals, in which ISFs are wider than those in Al, molecular dynamics or molecular statics (MS) is the method of choice. However, the accuracy of the calculated core structure from these methods depends on the reliability of the interatomic potential used and whether it was developed for defect calculations.^{14–16} For the same FCC metal, the same dislocation character, and the same measurement method, predictions for the ISF width can vary widely among atomistic studies.^{17–20}

At the other extreme lies classical linear elastic continuum dislocation theory, which neglects the atomic details of the core altogether and applies to the elastic continuum region outside the core. Presuming a dissociated or split core structure *a priori*, the ISF width is estimated based on a force balance between the linear elastic repulsion between the two partial dislocations and the attraction associated with γ_{isf} . It has the advantage of providing a quick and insightful estimation of the core width, but it can significantly deviate from the results based on atomistic simulations.¹⁴

More advanced continuum-based computational models, such as the generalized Peierls-Nabarro (GPN) model^{21–24} and the phase-field (PF) model,^{25–27} have also been employed to simulate the relaxation of a dislocation from its compact, perfect state into its low-energy dissociated structure. Two essential components included in these computational techniques are the linear elastic interactions between the Shockley partial dislocations, as in the classical model, and the nonlinear interactions between atoms across the glide plane. The latter is usually represented as a function relating the excess energy incurred as the two atomic planes are displaced relative to one another in the plane of glide. In practice, the possible shift vectors made available to the core calculation have varied, from solely those along the Burgers vector to those corresponding to all possible in-plane displacements. The energetic surface corresponding to all in-plane shift vectors is called the generalized stacking fault energy (GSFE) surface.

GPN-based and PF-based models have demonstrated that the relaxation process into a dissociated state is best predicted when the entire GSFE surface is taken into account. For instance, it was shown using GPN-based simulations that using two GSFE surfaces for Ni that have the same γ_{isf} but 16.7% difference in the unstable stacking fault energy (USFE), γ_{usf} , results in an 8.7% difference in the ISF width.²⁸ Linear elasticity theory, which uses only γ_{isf} , tends to predict a higher ISF width than GPN/PF models, especially when γ_{isf} is relatively small.^{26,29,30} Another recent study using PF-based dislocation models found that calculations of the ISF widths achieved much better agreement with those from atomistic calculations when the GSFE surface representation was accurate over the entire surface and not just at special local maxima or minima.³¹

Over the years, direct calculation of the entire GSFE surface is usually accomplished via MS, rather than DFT. Yet, as we have already alluded earlier, MS-based GSFE surfaces are sensitive to the interatomic potential used.³² Values for certain points on the

GSFE surface are found to disagree with DFT. In Al and Ni, for instance, γ_{isf} predicted by various embedded-atom method (EAM) potentials was shown to be one order of magnitude smaller than that based on DFT.³³ DFT is used to only calculate selected portions of the surface, usually the GSFE curves along the $\langle 112 \rangle$ and/or $\langle 110 \rangle$ directions, but not the entire surface. DFT has been used to calculate GSFE curves for Ag,^{30,34,35} Al,^{30,35–39} Au,^{30,34,35} Cu,^{30,34,35,38,39} Ir,^{30,34,35,37} Ni,^{30,34,35,38} Pb,^{34,35} Pd,^{30,34–37} Pt,^{30,34,35,37} and Rh.^{30,34,37} As one exception, Lu *et al.*⁴⁰ obtained 40 values on 1/12 of the entire GSFE surface for Al.

As an alternative to direct calculation of the entire surface, many works have elected to use DFT to calculate specific points on the surface and use them to build the entire GSFE surface via a continuous function. In particular, N_{fs} -term Fourier-series functions, with $N_{\text{fs}} = 2$ (Ref. 34), 6 (Ref. 23), 7 (Ref. 41), 8 (Ref. 42), or 11 (Ref. 31), have been used for pure FCC metals. In each function, the N_{fs} coefficients are fit to preselected N_{fs} GSFE values, usually the local minima or maxima. The Fourier-series functions represent those selected points reliably, but not necessarily the remaining points. Furthermore, unless the entire surface is given, it is unknown whether the preselected points correspond to the actual local maxima and minima.

In this paper, we use DFT to calculate the full GSFE surfaces of eight FCC transition metals, including Ag, Au, Cu, Ir, Ni, Pd, Pt, and Rh. We show that five metals can be described well by an 11-term Fourier-series function, for which we characterize and provide. We identify an anomalous local minimum in the GSFE surfaces in Ir and Rh, suggesting a possible high-stress-induced dissociated structure. The results reveal that the GSFE surface of Pt has a special characteristic of not exhibiting any well-defined maxima or minima, implying that its core would spread rather than dissociate. DFT-based GSFE surfaces for these common pure FCC metals can provide understanding of atomic bonding across crystallographic planes on which dislocations glide and enable continuum dislocation models to reliably predict dislocation core structures.⁴³

II. METHODS

All DFT calculations conducted in this study use VASP.⁴⁴ Within the framework of the projector augmented wave method,^{45,46} a pseudopotential is used for each metal to approximate the core electrons, and a plane wave basis is adopted for the valence electrons. Table I summarizes the numbers of valence electrons per atom and the cutoff energies E_{cut} for the plane-wave basis set. The exchange-correlation energy functional is approximated by the Perdew-Burke-Ernzerhof (PBE) formulation of the generalized gradient approximation (GGA).⁴⁷

For the electronic self-consistent loop, the residual minimization scheme with direct inversion in the iterative subspace is used, and the convergence is reached when the total free energy change and the band structure energy change between two steps are both smaller than 10^{-4} eV. The Brillouin zone is constructed by the Monkhorst-Pack scheme.⁴⁹ For correct handling of the Fermi surface, the Methfessel-Paxton smearing method⁵⁰ with a smearing width $\sigma = 0.2$ eV is employed, unless stated otherwise. Among the eight metals, spin-polarization is considered only for Ni,

TABLE I. A summary of two parameters for DFT calculations: the number of valence electrons per atom N_{ve} and the cutoff energy for the plane-wave basis set E_{cut} (in eV).

	Ag	Au	Cu	Ir	Ni^{NM}	Ni	Pd	Pt	Rh
N_{ve}	17	11	17	9		16	10	10	15
E_{cut}	446.8	344.91	552.97	316.3		551.98	376.39	345.42	371.11

where ferromagnetism is assumed. Results based on nonmagnetic Ni are denoted as Ni^{NM} .

For each metal, a periodic cell containing four atoms is used to determine the lattice parameter a_0 and elastic constants C_{11} , C_{12} , and C_{44} . The k -point mesh in these calculations is $11 \times 11 \times 11$. For a_0 , the cell size is varied, and for each size, the free energy without ionic relaxation is calculated. With this approach, a_0 corresponds to the cell size with the smallest free energy. The elastic constants are calculated via the energy-strain method provided in AELAS.⁵¹ The results are summarized in Table II.

For the GSFE surface calculations, a cell with lattice orientations of $x[\bar{1}\bar{1}2]$, $y[1\bar{1}1]$, and $z[\bar{1}\bar{1}0]$ is built containing 24 atoms, with two atoms on each (111) plane. In other words, the number of atomic layers, N_{al} , is 12. A vacuum region of 8 \AA is added to each cell along the y direction, creating a series of noninteracting slabs. Unless stated otherwise, $13 \times 1 \times 17$ k -points are adopted. Note that the smearing width σ is related to the k -point number. To ensure convergence of the GSFEs, for $\sigma = 0.2 \text{ eV}$ and $N_{al} = 12$, different k -point numbers and E_{cut} values are tested. Then, with fixed k -point number and E_{cut} value, different values of σ and N_{al} are tested in selected cases, which will be presented in Sec. III. We remark that in previous work, (i) $N_{al} = 12$ was found to be sufficiently large for selected GSFE values in ten FCC metals,³⁴ and (ii) $\sigma = 0.2 \text{ eV}$ was used to calculate selected GSFE values in nine FCC metals.³⁰

To obtain the GSFEs, the top six layers of atoms, in the y direction, are displaced with respect to the bottom six layers incrementally and independently along the x and z directions, until the displacements d_x and d_z reach the respective periodic lattice lengths $d_{x0} = \sqrt{6}a_0/2$ and $d_{z0} = \sqrt{2}a_0/2$. Following each displacement $[d_x, d_z]$, the top two and bottom two layers of atoms are fixed, while the remaining eight layers are allowed to relax along the y direction. The ionic relaxation stops when the total energy between two steps is smaller than 10^{-3} eV/atom .³⁹ The

GSFE surface is represented by the energies associated with a fine 101×65 grid of the $[d_x, d_z]$ displacements. Data for the GSFE surfaces in all eight metals are available in Materials Cloud.⁵²

III. RESULTS

As a way to check the DFT method and model, we first compare our results for Cu to those reported by prior DFT studies using the same PBE-GGA formulation of the exchange-correlation energy functional. Among the eight metals considered here, the fault energies for Cu are among the most extensively studied by DFT,^{30,34,35,38,39} and the structures of the dislocations in Cu have drawn considerable attention.^{53,54} Figure 1 presents the GSFE surface of Cu from our DFT calculations. As mentioned, prior GSFE calculations in Cu have not aimed to produce the entire surface, but rather slices of the surface lying within the region AGA' , which is illustrated in Fig. 1(d). This region contains key local minima and maxima related to the equilibrium core structure of dislocations in FCC systems. A perfect dislocation with Burgers vector AA' dissociates into two Shockley partial dislocations AG and GA' , i.e.,

$$\frac{a_0}{2}[\bar{1}10] = \frac{a_0}{6}[2\bar{1}1] + \frac{a_0}{6}[\bar{1}2\bar{1}]. \quad (1)$$

Based on a hard-sphere model of the atomic positions during the displacements,⁵ a local minimum would ideally exist at $d_{x0}/3$, where two adjacent hexagonal close-packed atomic layers form [see Fig. 1(b)]. The displacement is associated with the Shockley partial Burgers vector, and the corresponding GSFE value is the ISFE, γ_{isf} . In the displacement pathway along AG between 0 and $d_{x0}/3$, there exists a local maximum, which is the USFE, γ_{usf} . The displacement for γ_{usf} , denoted as d_{usf} , is ideally $d_{x0}/6$, according to the hard-sphere model of an FCC lattice.

TABLE II. A summary of the lattice parameter a_0 (in \AA) and elastic constants C_{11} , C_{12} , and C_{44} (in GPa), calculated by this work (DFT). Experimental measurements (Exp)⁴⁸ are also given for comparison.

	Method	Ag	Au	Cu	Ir	Ni^{NM}	Ni	Pd	Pt	Rh
a_0	DFT	4.153	4.157	3.634	3.873	3.514	3.519	3.942	3.968	3.831
	Exp	4.086	4.078	3.615	3.839		3.524	3.89	3.923	3.803
C_{11}	DFT	100.5	151.99	174.96	583.65	259.22	278.87	202.29	299.51	405.34
	Exp	122	191	169	580		247	221	347	413
C_{12}	DFT	85.25	134.16	121.57	234.36	172.74	158.83	151.32	225.36	183.1
	Exp	92	162	122	242		153	171	251	194
C_{44}	DFT	39.16	27.69	76.45	254.35	110.3	132.18	61.52	59.85	187.47
	Exp	45.5	42.2	75.3	256		122	70.8	76.5	184

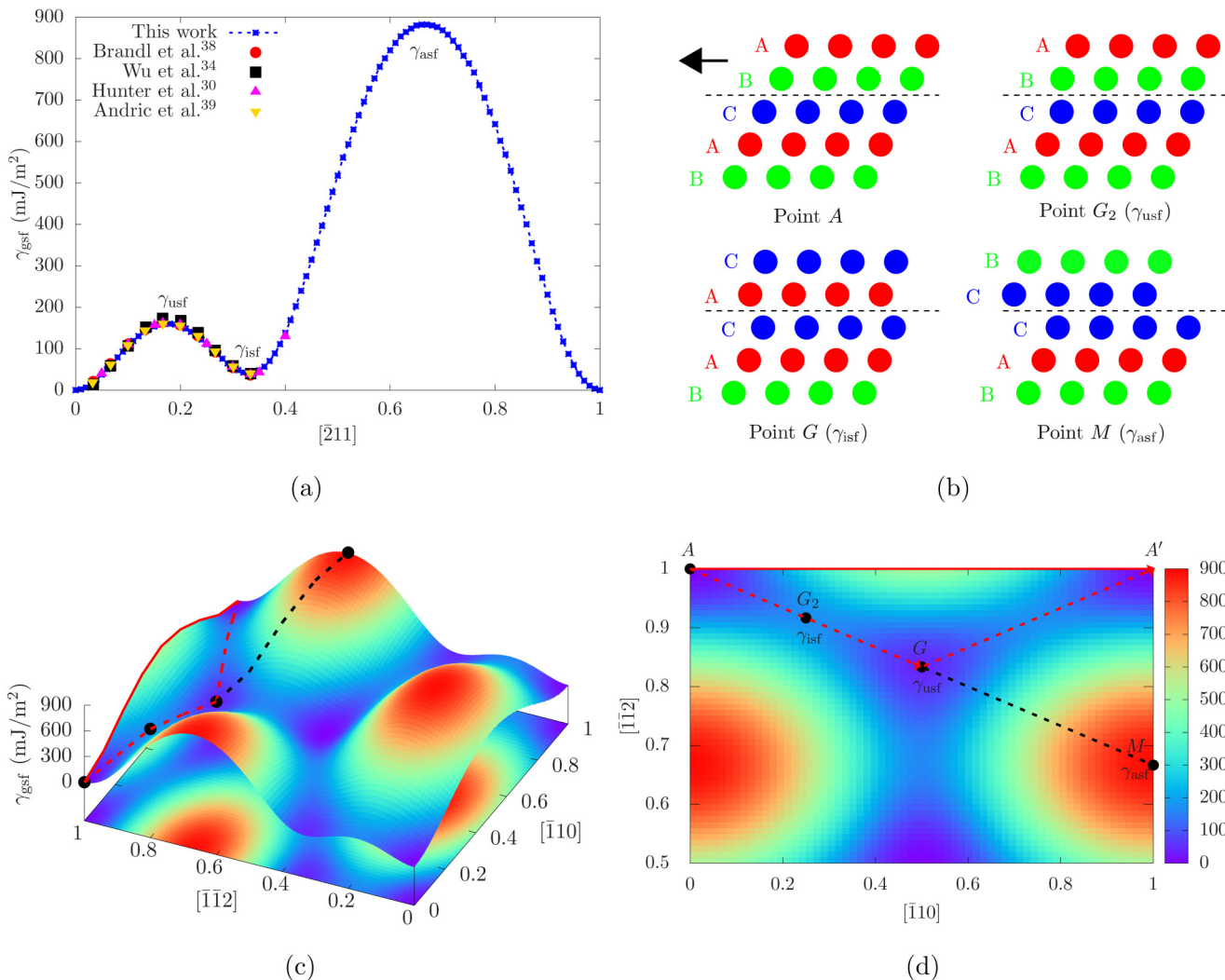


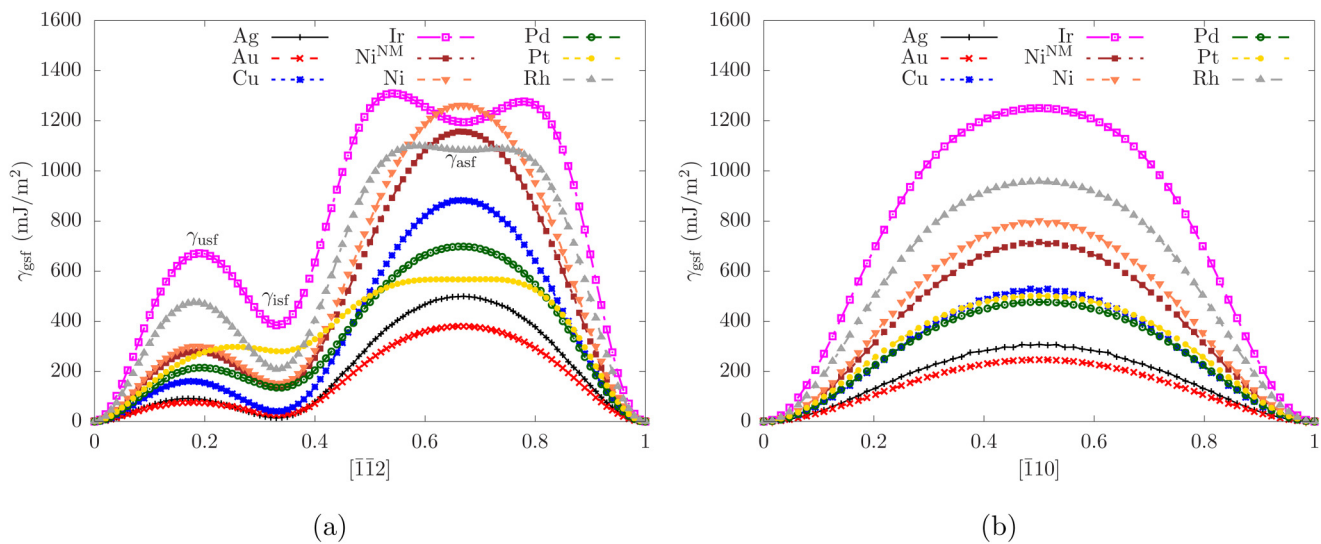
FIG. 1. Results based on DFT calculations in Cu. (a) Relaxed GSFE curves along the $\langle 211 \rangle$ direction, of which the portion between 0 and $0.4d_{x0}$ agrees with those of previous DFT calculations.^{30,34,38,39} (b) Illustrative atomic configurations for the four points (A, G_2 , G, and M) in (c) and (d); the dashed lines are the slip planes, with the atoms below fixed and the atoms above moved toward left as indicated by the arrow. (c) 3D relaxed GSFE surface on a (111) plane along both $[112]$ and $[110]$ directions. (d) is the projection of a portion of (c) onto the (111) plane. Note that the arrows AG and GA' point to the $[211]$ and $[121]$ directions, respectively.

Previous DFT calculations reported the portion of the $\langle 112 \rangle$ GSFE curve between 0 and $0.4d_{x0}$, which spans γ_{usf} and γ_{isf} .^{30,34,38,39} Figure 1(a) compares this part of the $\langle 112 \rangle$ GSFE curve from our calculations with those of others, showing excellent agreement. Common to the literature, the local maximum γ_{usf} is reached at $0.17d_{x0}$ in our DFT calculations, and the local minimum γ_{isf} occurs at $0.33d_{x0}$. Given the numerical resolution, $\pm 0.005d_{x0}$, we consider these two displacements the same as the hard-sphere model prediction, $d_{x0}/6$ and $d_{x0}/3$, respectively.

In Fig. 1(a), we also show the energies from our calculations corresponding to $\langle 112 \rangle$ in-plane displacements larger than $0.4d_{x0}$ and up to the full periodic length d_{x0} . This region of the $\langle 112 \rangle$ GSFE

curve was considered inaccessible by dislocations and was not studied in prior DFT studies. In the ideal GSFE surface, the $\langle 112 \rangle$ curve is expected to achieve a maximum at point M [Fig. 1(d)] for a shift of $2d_{x0}/3$, when two adjacent layers of atoms are perfectly aligned, wherein atoms lie directly on top of each other [Fig. 1(b)]. Hence, we term the GSFE value at M as the “aligned SFE”, denoted as γ_{asf} . Note that it was called by Lu and Kaxiras³⁵ as “run-one SFE”. Our calculations show that for Cu, γ_{asf} sits at the global maximum, as shown in Fig. 1(c).

Having demonstrated consistency with other DFT calculations in the literature, we proceed to examine the full γ -surface for all eight metals, with particular focus on their $\langle 110 \rangle$ curves and $\langle 112 \rangle$

FIG. 2. Relaxed GSFE curves along the $\langle 112 \rangle$ and $\langle 110 \rangle$ directions for all eight metals.

GSFE curves. Figure 2 presents the GSFE curves for all eight metals along the $\langle 110 \rangle$ and $\langle 112 \rangle$ directions, respectively. For the $\langle 110 \rangle$ curve, it is expected that the peak energy, γ_{110}^P , would correspond to a displacement at the halfway point, at $d_{x0}/2$. Indeed, a maximum is reached in all metals at $d_{x0}/2$, and the GSFE values are symmetric with respect to it. The peak value γ_{110}^P varies substantially, being highest for Ir and lowest for Au.

More studied in the literature are the $\langle 112 \rangle$ curves. The pathway AG possesses the local minimum γ_{isf} , and the local maximum along the $\langle 112 \rangle$ path, γ_{usf} , is much smaller than γ_{110}^P . Thus, displacements along the $\langle 112 \rangle$ pathway are likely to determine the behavior and structure of the dislocation. In all metals, the local minimum γ_{isf} is achieved at $d_{x0}/3$. Our results that Ni has higher γ_{isf} and γ_{usf} than Ni^{NM} are consistent with a prior DFT calculation.³⁸ Two more findings are worth noting. First, the $\langle 112 \rangle$ curve for Pt bears no well-defined maximum or minimum over the entire periodic length. Second, the $\langle 112 \rangle$ displacement to reach γ_{usf} , d_{usf} , differs substantially among the metals, and all metals (except Ag and Cu) deviate from the hard-sphere value of $d_{x0}/6$. The values of γ_{usf} and d_{usf} are summarized in Table III. The value for d_{usf} for Ag and Cu is the

closest to the ideal one and the smallest, while that for Pt is the largest.

For the $\langle 112 \rangle$ curve, the GSFE values corresponding to displacements larger than $0.4d_{x0}$ are significantly larger than those in region AGA'. We find that, in addition to Cu [Fig. 1(c)], γ_{asf} in four other FCC metals (Ag, Au, Ni, and Pd) correspond to the global maximum, as shown in Fig. 3, achieved at $2d_{x0}/3$. Pt, as shown in Fig. 4, does not exhibit well-defined extrema, particularly at γ_{asf} . In the two remaining metals (Ir and Rh), we observe an interesting finding that γ_{asf} sits at a local minimum. To better highlight this energy well, Figs. 5(a) and 5(b) present the entire GSFE surface for Ir and Rh.

IV. DISCUSSION

A. Parameterization

In this section, we consider parameterizations of these fully calculated GSFE surfaces via an 11-term Fourier-series continuous function.³¹ This type of functions can be directly used in continuum models for static and dynamic dislocation studies and can offer insight and understanding of dislocation energetics. The

TABLE III. A summary of the USFE γ_{usf} (in mJ/m²), the displacement d_{usf} (in d_{x0}) for γ_{usf} , ISFE γ_{isf} (in mJ/m²), aligned SFE γ_{asf} (in mJ/m²), and the peak GSFE value along the $\langle 110 \rangle$ curve, γ_{110}^P (in mJ/m²).

	Ag	Au	Cu	Ir	Ni^{NM}	Ni	Pd	Pt	Rh
γ_{usf}	92.01	76.68	160.52	671.66	279.69	300.89	214.93	297.92	475.34
d_{usf}	0.17	0.18	0.17	0.19	0.19	0.19	0.2	0.25	0.18
γ_{isf}	14.49	26.79	41.83	385.87	139.01	152.13	135.54	280.87	208.67
γ_{asf}^P	499.26	380	891.28	1194.4	1157.75	1262.14	698.69	566.96	1077.54
γ_{110}^P	307.39	246.57	519.05	1250.63	716.3	801.47	476.98	501.97	958.3

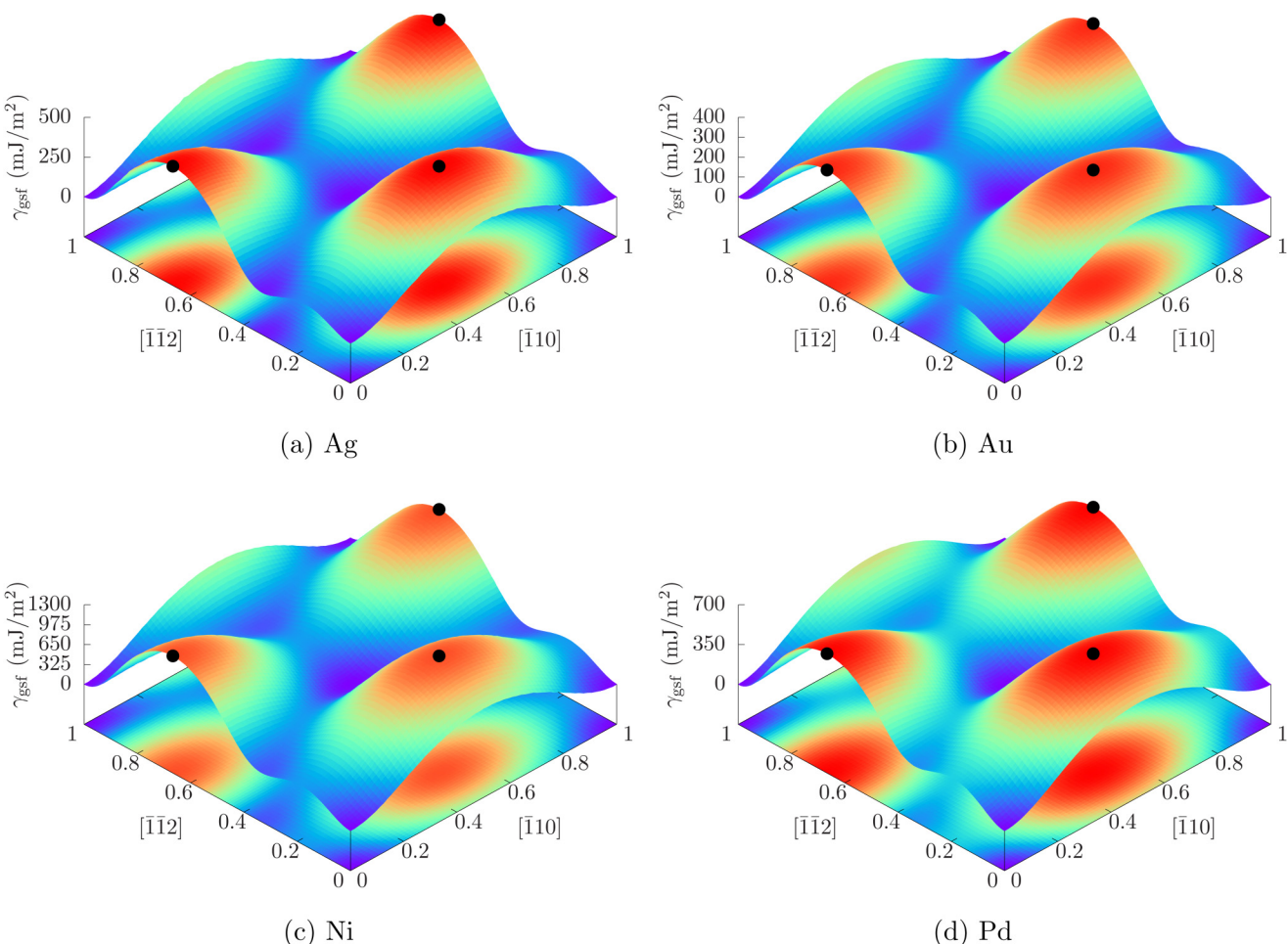


FIG. 3. Relaxed GSFE surfaces in Ag, Au, Ni, and Pd, for which γ_{asf} , denoted by the black filled circles, sits at a local maximum, which is also the global maximum.

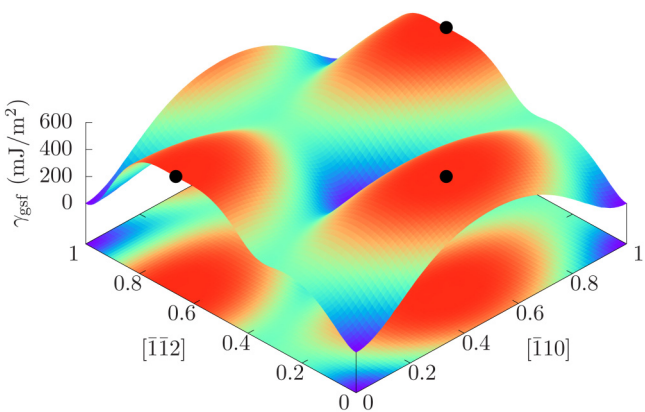


FIG. 4. Relaxed GSFE surface in Pt for which γ_{asf} is denoted by the black filled circles. There are no well-defined extrema.

Fourier series function for the GSFE surface takes the form

$$\begin{aligned} \gamma_{\text{gsf}} = & c_0 + c_1 [\cos(2pd_x) + \cos(pd_x + qd_z) + \cos(py - qz)] \\ & + c_2 [\cos(2qd_z) + \cos(3pd_x + qd_z) + \cos(3pd_x - qd_z)] \\ & + c_3 [\cos(4pd_x) + \cos(2pd_x + 2qd_z) + \cos(2pd_x - 2qd_z)] \\ & + c_4 [\cos(pd_x + 3qd_z) + \cos(pd_x - 3qd_z) + \cos(4pd_x + 2qd_z) \\ & \quad + \cos(4pd_x - 2qd_z) + \cos(5pd_x + qd_z) + \cos(5pd_x - qd_z)] \\ & + c_5 [\sin(2pd_x) - \sin(pd_x + qd_z) - \sin(pd_x - qd_z)] \\ & + c_6 [\sin(4pd_x) - \sin(2pd_x + 2qd_z) - \sin(2pd_x - 2qd_z)] \\ & + c_7 [\cos(6pd_x) + \cos(3pd_x + 3qd_z) + \cos(3pd_x - 3qd_z)] \\ & + c_8 [\cos(8pd_x) + \cos(4pd_x + 4qd_z) + \cos(4pd_x - 4qd_z)] \\ & + c_9 [\cos(4qd_z) + \cos(6pd_x + 2qd_z) + \cos(6pd_x - 2qd_z)] \\ & + c_{10} [\cos(6qd_z) + \cos(9pd_x + 3qd_z) + \cos(9pd_x - 3qd_z)], \end{aligned} \tag{2}$$

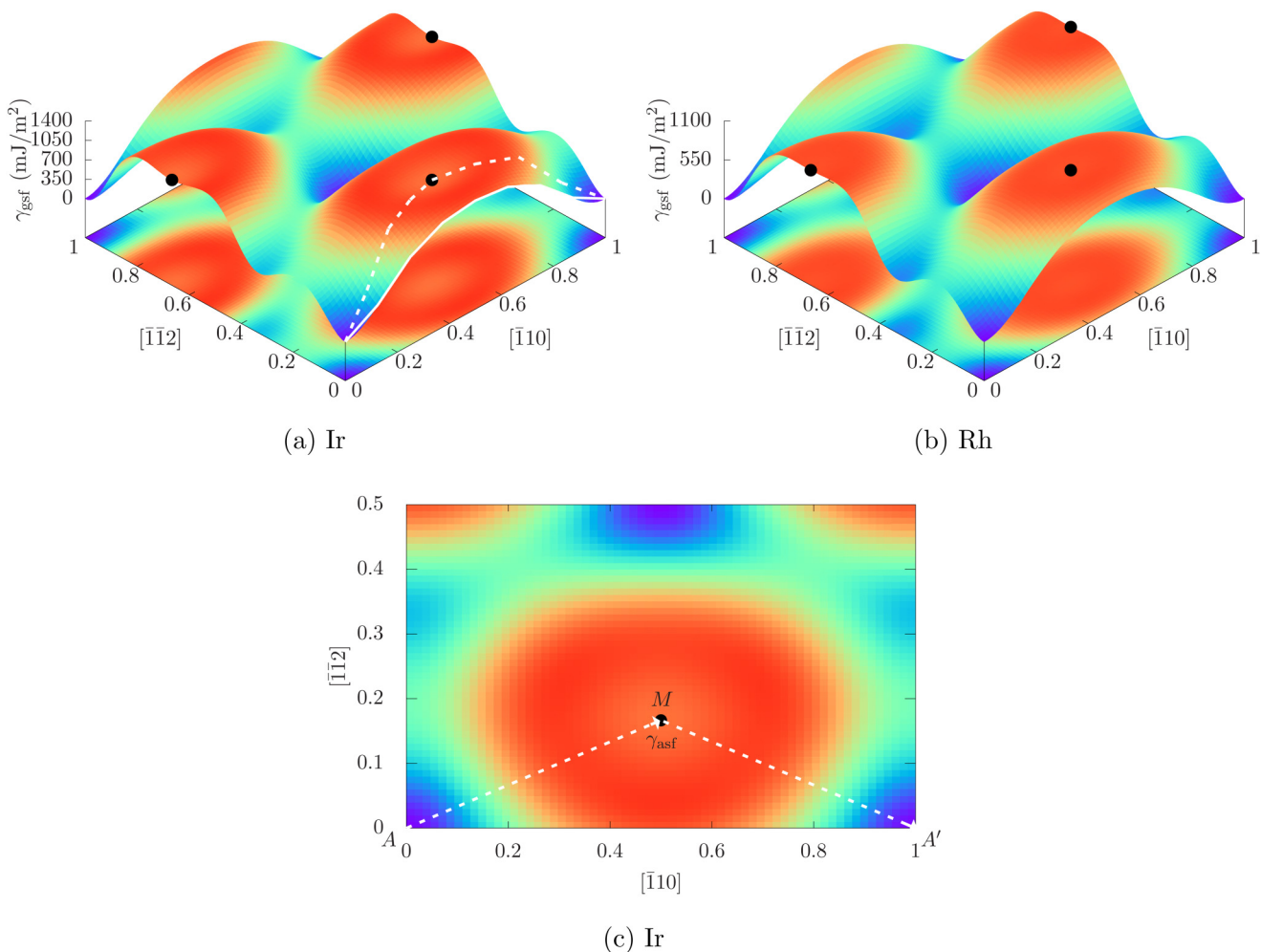


FIG. 5. (a) and (b) Relaxed GSFE surfaces in Ir and Rh for which γ_{ASF} is denoted by the black filled circles and sits at a local minimum. (c) is the projection of a portion of (a) onto the (111) plane.

where $p = (2\sqrt{6}/3)\pi/a_0$ and $q = 2\sqrt{2}\pi/a_0$ are magnitudes of the reciprocal lattice vectors. The 11 coefficients c_i are presented in Table IV by fitting the equation above to the 11 GSFE values as described in Ref. 31.

The 11-term Fourier-series function is found to provide an accurate representation for the GSFE surfaces for five metals: Ag, Au, Cu, Ni, and Pd. For Pt, the fit is not as perfect but reasonable, as will be discussed shortly. For Ir and Rh, it fails to capture the local minimum at point M , the origin of which we examine further below. Thus, for these three transition FCC metals, Pt, Ir, and Rh, direct DFT calculations of the GSFE curves are preferred over analytic approximations.

B. Pt

The unique energetic landscape of the entire GSFE surface of Pt shows that Pt has a distinct and more complex bonding

structure than other metals. To assess the effects of the smearing width σ and the number of atomic layers N_{al} , we vary σ from 0.05 eV to 0.4 eV and N_{al} from 6 to 15. Results, presented in Fig. 6, demonstrate that use of $\sigma = 0.2$ eV and $N_{\text{al}} = 12$ in these calculations is appropriate for Pt.

To further validate the result, we sought another method, in which the exchange-correlation functional in the DFT calculations is approximated by GGA+ U^{56} rather than GGA. Compared with GGA, GGA+ U is considered to more accurately describe the localization of d orbitals of transition metals. It does require, however, at least one additional energy term that is usually unknown *a priori*.⁵⁷ Here, for the GGA+ U calculation, we aim to characterize a single effective Hubbard correction, U_{eff} , for the on-site Coulomb interactions of localized electrons in the d orbitals. For each metal, we determine its value by fitting the GGA+ U -based lattice parameter a_0 to that measured in experiments.⁴⁸ As shown in Fig. 7(a), $U_{\text{eff}} = 3.357$ eV

TABLE IV. A summary of the 11 coefficients c_i , in units of mJ/m^2 , in Eq. (2).

	Ag	Au	Cu	Ir	Ni ^{NM}	Ni	Pd	Pt	Rh
c_0	222.77	177.08	383.24	932.83	530.09	589.67	360.73	385.07	708.48
c_1	-60.11	-48.06	-107.47	-185.45	-146.6	-161.16	-93.69	-93.85	-151.06
c_2	-16.8	-13.39	-22.86	-131	-36.91	-42.21	-27.91	-34.63	-90.14
c_3	3.21	3.42	3.82	11.95	3.97	5.07	1.74	1.71	9.2
c_4	0.01	-0.47	0.07	-0.77	-0.01	-0.18	-0.14	-0.59	-0.3
c_5	-99.9	-75.8	-172.98	-189.38	-208.12	-229.7	-117.38	-73.57	-189.92
c_6	-6.6	-7.83	-9.5	-33.78	-12.06	-16.07	-9	-18.51	-22.71
c_7	0.41	0.91	-0.04	5.95	5.63	4.29	2.82	4.48	3.04
c_8	0.02	0.38	-0.12	-0.53	-0.52	0.03	-0.45	-0.82	-0.43
c_9	-0.89	-1.18	-0.95	-9.72	-2.1	-2.08	-2.31	-3.82	-5.38
c_{10}	-0.12	-0.16	-0.27	-0.6	-0.15	-0.12	-0.18	-0.24	-0.79

provides a good fit for Pt. The two calculations for Pt are compared in Fig. 7(b), where it is seen that for Pt, γ_{asf} from GGA+U provides generally different fault energies and even shallower maxima and minima, compared to the $\langle 112 \rangle$ GSFE curve based on GGA.

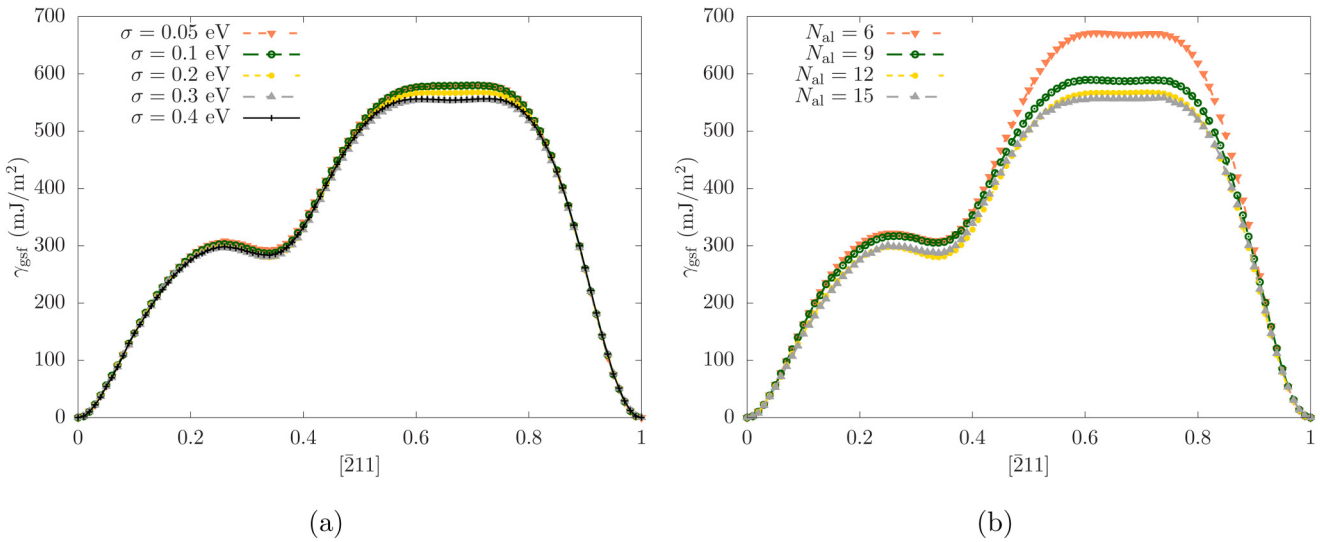
Figure 8 presents the GSFE curves in Pt along the $\langle 112 \rangle$ and $\langle 110 \rangle$ directions using DFT, the 11-term Fourier-series representation,³¹ and several EAM potentials.^{58–62} It is found that (i) all EAM potentials predict γ_{isf} less than 50% of the DFT-calculated value; (ii) while one EAM potential⁶¹ gives a reasonably good γ_{usf} value, none correctly predict the large d_{usf} ; and (iii) although the 11-term Fourier-series function captures the general shape of the DFT-calculated curve, it predicts a larger convexity at $2d_{x0}/3$ along the $\langle 112 \rangle$ direction and an incorrect local minimum at $d_{z0}/2$ on the $\langle 110 \rangle$ curve.

Some of these anomalies in the $\langle 112 \rangle$ GSFE curve of Pt, namely, the unusually large $d_{\text{usf}} = d_{x0}/4$ and the lack of a well-defined local minimum at γ_{isf} , have been reported in prior DFT calculations.^{30,34,35}

These oddities were attributed to a unique change in the interatomic bonding in the ISF, which were revealed by a valence charge density difference (VCDD) analysis.³⁰ Furthermore, the lack of a deep local minimum in the $\langle 112 \rangle$ GSFE curve, and the entire surface, suggests that, unlike the other metals, dislocation dissociation is not favorable. Incorporating the DFT-informed GSFE surface into the energy functional, a PF-based model indicated that the equilibrium dislocation core did not involve a dissociation but rather a spreading within its $\{111\}$ glide plane.³⁰ Taken together, to date, for Pt, direct calculation of the entire GSFE surface using DFT is preferred over using semiempirical interatomic potentials or Fourier-series representations.

C. Ir and Rh

As mentioned, in Ir and Rh, γ_{asf} sits at a local minimum. To validate the result, we again vary σ from 0.05 to 0.4 eV and N_{al} from 6 to 15. Figure 9 shows that our choices of $\sigma = 0.2$ eV and

**FIG. 6.** Relaxed GSFE curves along the $\langle 112 \rangle$ direction for Pt, with (a) $N_{\text{al}} = 12$ but different smearing width σ and (b) $\sigma = 0.2$ eV but different number of atomic layers N_{al} .

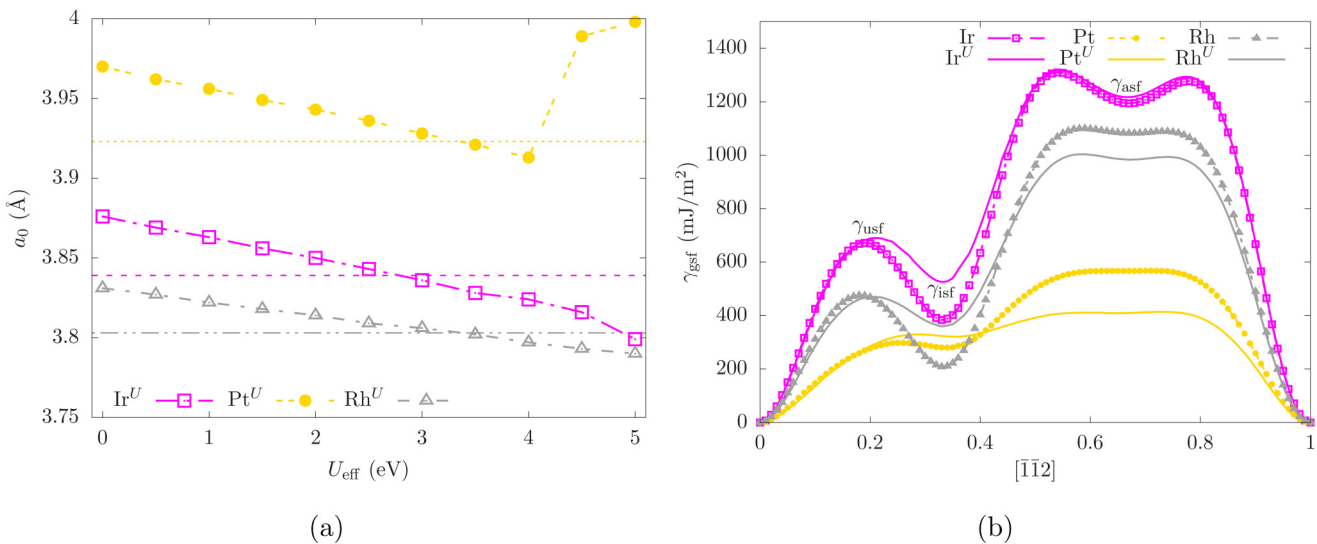


FIG. 7. (a) Lattice parameter, a_0 , predicted by DFT calculations with the exchange-correlation energy functional approximated by GGA+ U , with respect to U_{eff} . Experimental values of a_0 , as summarized in Table II, are shown as horizontal dashed lines. (b) Relaxed GSFE curves along the $\langle 112 \rangle$ direction for Ir, Pt, and Rh, while the exchange-correlation energy functional approximated by GGA (symbols) or GGA+ U (solid line).

$N_{\text{al}} = 12$ are appropriate for Ir. As another check, for Ir and Rh, we recalculated the entire $\langle 112 \rangle$ GSFE curves using DFT with the exchange-correlation functional approximated by GGA+ U .⁵⁶ Using the same method for characterizing U_{eff} already described, we determine that $U_{\text{eff}} = 2.786$ and 3.375 eV, respectively, for Ir and Rh. We observe in Fig. 7(b) that with GGA+ U , γ_{asf} still sits at a local minimum of the $\langle 112 \rangle$ GSFE curve. Agreement in this

particular feature suggests that the anomalous local minimum at γ_{asf} for Ir and Rh is not the result of an inaccurate description of the d -orbital localization via GGA.

The reason for the anomaly at γ_{asf} may lie in a change in the electronic or atomic structure in the aligned faulted region that arises for these two metals but not the others. To expose the change in the electronic structure, we calculated the VCDD in the

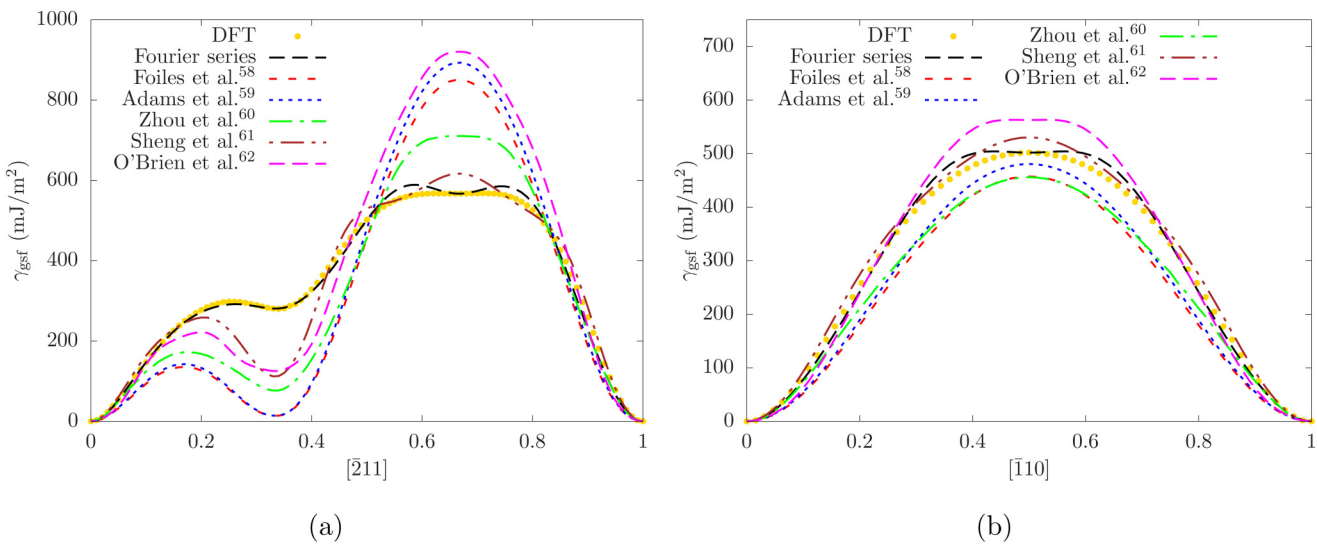


FIG. 8. Relaxed GSFE curves along the $\langle 112 \rangle$ and $\langle 110 \rangle$ directions for Pt using DFT, DFT-informed 11-term Fourier-series function [Eq. (2)], and several EAM potentials.^{58–62}

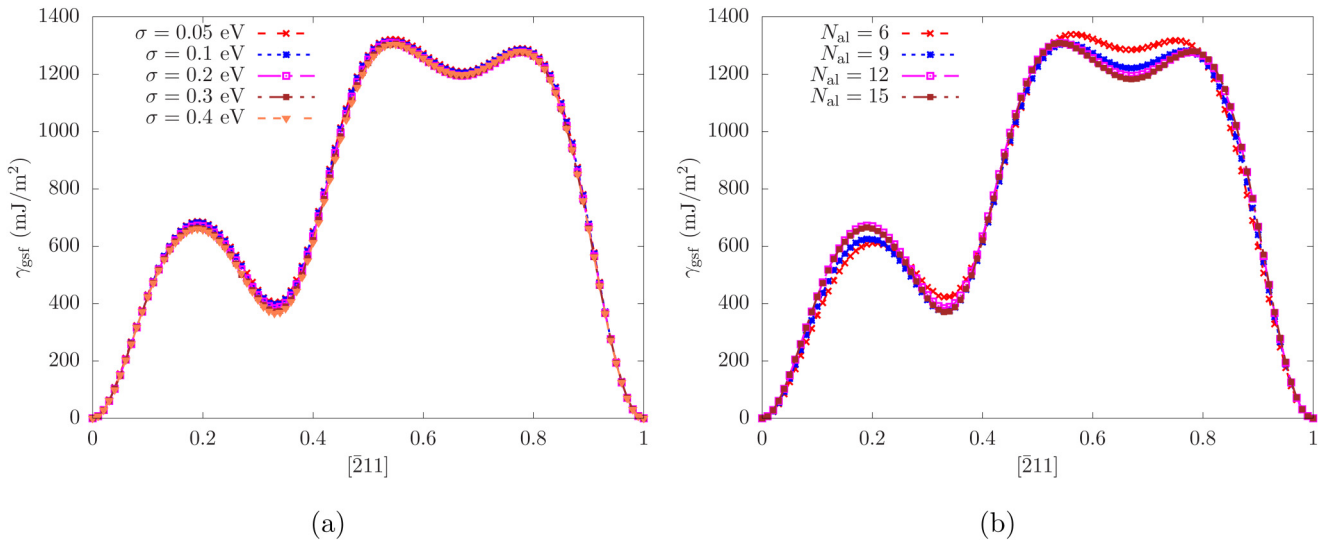


FIG. 9. Relaxed GSFE curves along the $\langle 112 \rangle$ direction for Ir, with (a) $N_{\text{al}} = 12$ but different smearing width σ and (b) $\sigma = 0.2 \text{ eV}$ but different number of atomic layers N_{al} .

aligned fault at point M for all eight metals. The VCDD maps between the unfaulted and faulted regions produced are similar; that is, no unique change in the symmetry and directionality of the charge transfer from the unfaulted to the faulted region emerged for Ir and Rh. Therefore, alterations in the charge transfer at point M do not explain the anomalous local minimum seen in these two metals.

Last, we examine the atomic displacement associated with point M . Recall that the GSFE surfaces are obtained after energy

minimization during which atoms were allowed to move along the y direction. To quantify the atomic displacements during the relaxation, we revisit the unrelaxed $\langle 112 \rangle$ GSFE curves, which are shown in Fig. 10(a). Significantly, we find that a global maximum lies at point M for all metals. The difference between the relaxed and unrelaxed curves, particularly at point M , indicates that additional local atomic displacements took place to accommodate fault formation at point M . Here, to determine whether a special set of

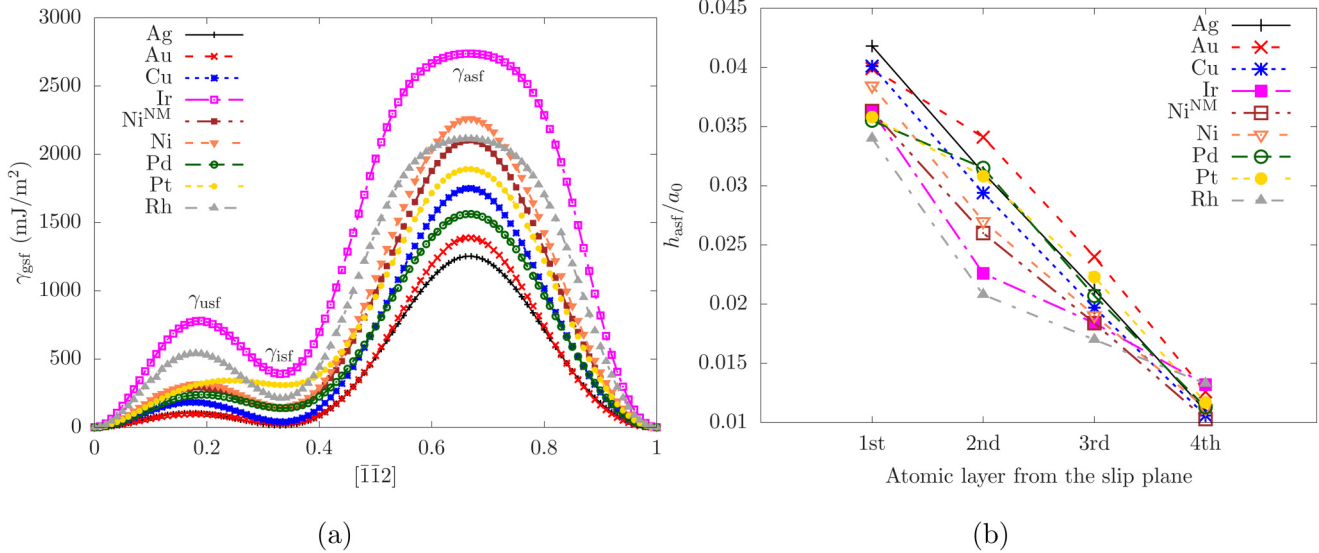


FIG. 10. (a) Unrelaxed GSFE curves along the $\langle 112 \rangle$ direction for all eight metals. (b) The atomic displacement h_{asf} at point M during relaxation along the glide plane normal.

displacements occurs in forming the fault at point M , we further study in Fig. 10(b) the atomic displacements involved during relaxation at point M in the nearest four atomic planes for all eight metals. The analysis shows that, in Ir and Rh, the two atomic layers that are immediately adjacent to the glide plane have been significantly displaced compared to the third and fourth layers from the glide plane. Unlike all other metals, large, local atomic displacements occurred in Ir and Rh to accommodate the alignment of two adjacent $\{111\}$ planes at point M .

The sufficiently deep local minimum at M indicates a possible dissociation reaction to an extended dislocation structure that would take place in Ir and Rh, but not in the other metals. A full dislocation AA' would dissociate into two Shockley partial dislocations AM and MA' , i.e.,

$$\frac{a_0}{2} [\bar{1}\bar{1}0] = \frac{a_0}{6} [\bar{1}2\bar{1}] + \frac{a_0}{6} [\bar{2}\bar{1}1]. \quad (3)$$

The ISF width associated with this reaction would be much smaller than that associated with the creation of an ISF at γ_{ISF} . For an edge dislocation in Rh, for instance, linear elasticity theory predicts that the ISF widths following Eqs. (1) and (3) are, respectively, $9b$ and $1.74b$. Furthermore, the former reaction occurs under no stress, whereas the latter would only likely occur when the dislocation is subject to shear stresses that are sufficiently large to overcome the energy barriers between point A and point M .

V. CONCLUSIONS

In this paper, we use DFT to calculate the (111) GSFE surfaces of eight FCC transition metals, including Ag, Au, Cu, Ir, Ni, Pd, Pt, and Rh. Analysis of the $\langle 112 \rangle$ GSFE curves finds that the displacements corresponding to the USFE are larger than the ideal value for all eight metals except Ag and Cu, with Pt having the largest displacement. The GSFE surface of Pt does not possess well-defined local maxima and minima, suggesting that its dislocation core does not dissociate but spreads in the glide plane. In addition, at a $\langle 112 \rangle$ displacement $2d_{x_0}/3$, at which two adjacent planes would geometrically align, an anomalous local minimum occurs for Ir and Rh, suggesting the existence of a novel dissociated dislocation structure. This anomaly is shown to be a result of special, relatively large localized atomic displacements, taking place to accommodate the alignment that does not occur in the other metals. Based on these surface calculations, a Fourier-series parameterization is tested and shown to offer an excellent continuous function representation for five of these metals, Ag, Au, Cu, Ni, and Pd. The results of these analyses and the GSFE surfaces can provide insight and benefit continuum modeling of dislocations, such as the GPN/PF-based modeling, which requires reliable GSFE surfaces as input.^{23,26–31,41}

ACKNOWLEDGMENTS

We thank Dr. Xiangguo Li for helpful discussions. The authors gratefully acknowledge support from the Office of Naval Research under contract ONR BRC Grant No. N00014-18-1-2392. S.X. also gratefully acknowledges support in part by the Elings Prize Fellowship in Science offered by the California NanoSystems Institute on the UC Santa Barbara campus. Use was made of computational facilities

purchased with funds from the National Science Foundation (NSF) (No. CNS-1725797) and administered by the Center for Scientific Computing (CSC). The CSC is supported by the California NanoSystems Institute and the Materials Research Science and Engineering Center (MRSEC; NSF DMR 1720256) at UC Santa Barbara. This work used the Extreme Science and Engineering Discovery Environment (XSEDE), which is supported by the National Science Foundation (Grant No. ACI-1053575).

REFERENCES

- ¹A. G. Crocker, M. Doneghan, and K. W. Ingle, *Philos. Mag. A* **41**, 21 (1980).
- ²A. V. Granato, *Phys. Rev. Lett.* **68**, 974 (1992).
- ³J. A. Venables, *Philos. Mag.* **6**, 379 (1961).
- ⁴V. B. Shenoy, R. V. Kukta, and R. Phillips, *Phys. Rev. Lett.* **84**, 1491 (2000).
- ⁵D. Hull and D. J. Bacon, *Introduction to Dislocations*, 5th ed. (Butterworth-Heinemann, 2011).
- ⁶J. J. Hauser and B. Chalmers, *Acta Metall.* **9**, 802 (1961).
- ⁷C. A. Bronkhorst, S. R. Kalidindi, and L. Anand, *Philos. Trans. R. Soc. Lond. A* **341**, 443 (1992).
- ⁸V. Vitek, *Prog. Mater. Sci.* **36**, 1 (1992).
- ⁹R. M. J. Cotterill and M. Doyama, *Phys. Rev.* **145**, 465 (1966).
- ¹⁰M. Doyama and R. M. J. Cotterill, *Phys. Rev.* **150**, 448 (1966).
- ¹¹M. S. Duesbery, *Model. Simul. Mater. Sci. Eng.* **6**, 35 (1998).
- ¹²M. Iyer, B. Radhakrishnan, and V. Gavini, *J. Mech. Phys. Solids* **76**, 260 (2015).
- ¹³S. Das and V. Gavini, *J. Mech. Phys. Solids* **104**, 115 (2017).
- ¹⁴J. A. Moriarty, V. Vitek, V. V. Bulatov, and S. Yip, *J. Comput.-Aided Mater. Des.* **9**, 99 (2002).
- ¹⁵S. Xu, J. K. Startt, T. G. Payne, C. S. Deo, and D. L. McDowell, *J. Appl. Phys.* **121**, 175101 (2017).
- ¹⁶S. Xu, Y. Su, and S. Z. Chavoshi, *Mater. Res. Express* **5**, 016523 (2018).
- ¹⁷S. G. Srinivasan, X. Z. Liao, M. I. Baskes, R. J. McCabe, Y. H. Zhao, and Y. T. Zhu, *Phys. Rev. Lett.* **94**, 125502 (2005).
- ¹⁸S. Zhao, Y. N. Osetsky, and Y. Zhang, *J. Alloys Compd.* **701**, 1003 (2017).
- ¹⁹N. Burberry, R. Das, and W. G. Ferguson, *Comput. Mater. Sci.* **137**, 39 (2017).
- ²⁰J. Cho, T. Junge, J.-F. Molinari, and G. Anciaux, *Adv. Model. Simul. Eng. Sci.* **2**, 12 (2015).
- ²¹G. Schoeck, *Philos. Mag. A* **69**, 1085 (1994).
- ²²V. V. Bulatov and E. Kaxiras, *Phys. Rev. Lett.* **78**, 4221 (1997).
- ²³X. Xiang, H. Wei, P. Ming, and W. E, *Acta Mater.* **56**, 1447 (2008).
- ²⁴G. Liu, X. Cheng, J. Wang, K. Chen, and Y. Shen, *Sci. Rep.* **7**, 43785 (2017).
- ²⁵Y. U. Wang, Y. M. Jin, A. M. Cuitiño, and A. G. Khachaturyan, *Acta Mater.* **49**, 1847 (2001).
- ²⁶S. Xu, L. Smith, J. R. Mianroodi, A. Hunter, B. Svendsen, and I. J. Beyerlein, *Model. Simul. Mater. Sci. Eng.* **27**, 074004 (2019).
- ²⁷Y. Su, S. Xu, and I. Beyerlein, *Model. Simul. Mater. Sci. Eng.* **27**, 084001 (2019).
- ²⁸G. Schoeck, *Acta Mater.* **54**, 4865 (2006).
- ²⁹A. Hunter, R. F. Zhang, I. J. Beyerlein, T. C. Germann, and M. Koslowski, *Model. Simul. Mater. Sci. Eng.* **21**, 025015 (2013).
- ³⁰A. Hunter, R. F. Zhang, and I. J. Beyerlein, *J. Appl. Phys.* **115**, 134314 (2014).
- ³¹S. Xu, J. R. Mianroodi, A. Hunter, I. J. Beyerlein, and B. Svendsen, *Philos. Mag.* **99**, 1400 (2019).
- ³²S. Xu, L. Xiong, Y. Chen, and D. L. McDowell, *JOM* **69**, 814 (2017).
- ³³J. A. Zimmerman, H. Gao, and F. F. Abraham, *Model. Simul. Mater. Sci. Eng.* **8**, 103 (2000).
- ³⁴X.-Z. Wu, R. Wang, S.-F. Wang, and Q.-Y. Wei, *Appl. Surf. Sci.* **256**, 6345 (2010).
- ³⁵Z. H. Jin, S. T. Dunham, H. Gleiter, H. Hahn, and P. Gumbsch, *Scr. Mater.* **64**, 605 (2011).
- ³⁶J. Hartford, B. von Sydow, G. Wahnström, and B. I. Lundqvist, *Phys. Rev. B* **58**, 2487 (1998).
- ³⁷J. Cai, F. Wang, C. Lu, and Y. Y. Wang, *Phys. Rev. B* **69**, 224104 (2004).

- ³⁸C. Brandl, P. M. Derlet, and H. Van Swygenhoven, *Phys. Rev. B* **76**, 054124 (2007).
- ³⁹P. Andric, B. Yin, and W. A. Curtin, *J. Mech. Phys. Solids* **122**, 262 (2019).
- ⁴⁰G. Lu, N. Kioussis, V. V. Bulatov, and E. Kaxiras, *Phys. Rev. B* **62**, 3099 (2000).
- ⁴¹G. Schoeck, *Philos. Mag. A* **81**, 1161 (2001).
- ⁴²Y.-M. Juan and E. Kaxiras, *Philos. Mag. A* **74**, 1367 (1996).
- ⁴³P. Tu, Y. Zheng, C. Zhuang, X. Zeng, and H. Zhu, *Comput. Mater. Sci.* **159**, 357 (2019).
- ⁴⁴G. Kresse and J. Furthmüller, *Phys. Rev. B* **54**, 11169 (1996).
- ⁴⁵P. E. Blöchl, *Phys. Rev. B* **50**, 17953 (1994).
- ⁴⁶G. Kresse and D. Joubert, *Phys. Rev. B* **59**, 1758 (1999).
- ⁴⁷J. P. Perdew, K. Burke, and M. Ernzerhof, *Phys. Rev. Lett.* **77**, 3865 (1996).
- ⁴⁸*Springer Handbook of Materials Data*, 2nd ed., Springer Handbooks, edited by H. Warlimont and W. Martienssen (Springer International Publishing, 2018).
- ⁴⁹H. J. Monkhorst and J. D. Pack, *Phys. Rev. B* **13**, 5188 (1976).
- ⁵⁰M. Methfessel and A. T. Paxton, *Phys. Rev. B* **40**, 3616 (1989).
- ⁵¹S. H. Zhang and R. F. Zhang, *Comput. Phys. Commun.* **220**, 403 (2017).
- ⁵²Y. Su, S. Xu, and I. J. Beyerlein, Materials Cloud Archive (2019), <https://archive.materialscloud.org/2019.0041/>.
- ⁵³L. Lu, X. Chen, X. Huang, and K. Lu, *Science* **323**, 607 (2009).
- ⁵⁴Y. Chen, K. Y. Yu, Y. Liu, S. Shao, H. Wang, M. A. Kirk, J. Wang, and X. Zhang, *Nature Commun.* **6**, 7036 (2015).
- ⁵⁵G. Lu and E. Kaxiras, *Phys. Rev. Lett.* **89**, 105501 (2002).
- ⁵⁶V. I. Anisimov, J. Zaanen, and O. K. Andersen, *Phys. Rev. B* **44**, 943 (1991).
- ⁵⁷S. L. Dudarev, G. A. Botton, S. Y. Savrasov, C. J. Humphreys, and A. P. Sutton, *Phys. Rev. B* **57**, 1505 (1998).
- ⁵⁸S. M. Foiles, M. I. Baskes, and M. S. Daw, *Phys. Rev. B* **33**, 7983 (1986).
- ⁵⁹J. B. Adams, S. M. Foiles, and W. G. Wolfer, *J. Mater. Res.* **4**, 102 (1989).
- ⁶⁰X. W. Zhou, R. A. Johnson, and H. N. G. Wadley, *Phys. Rev. B* **69**, 144113 (2004).
- ⁶¹H. W. Sheng, M. J. Kramer, A. Cadien, T. Fujita, and M. W. Chen, *Phys. Rev. B* **83**, 134118 (2011).
- ⁶²C. J. O'Brien, C. M. Barr, P. M. Price, K. Hattar, and S. M. Foiles, *J. Mater. Sci.* **53**, 2911 (2018).